Radar and Data Communication Fusion with UWB-OFDM Software-Defined System

Dmitriy Garmatyuk
Department of Electrical and Computer Engineering
Miami University
Oxford, OH, USA
garmatd@muohio.edu

Kyle Kauffman
Department of Electrical and Computer Engineering
Miami University
Oxford, OH, USA
kauffmkj@muohio.edu

***Abstract*—This paper describes the architecture, testing methodology and experimental results of the software-defined ultra-wideband system built at Miami University. To achieve broadband data communication capability, spectrum-efficient OFDM method of modulation was chosen. The radar functionality using the same OFDM-coded pulses was implemented as well, and tested in short-range experiments. The system operates in X-band with a total transmit bandwidth of 1 GHz. Range resolution of 0.30 meters and data communication capability at approximately 57 Mb/s were established and the system was shown to be able to operate in either mode without any hardware adjustments. This concept may prove extremely useful in high-resolution radar sensor network scenarios.**

Keywords-UWB radar; OFDM; software-defined radar; dual-use system

I. INTRODUCTION

The concept of miniaturized, potentially dual-use (radar/communication), high-resolution all-weather imaging sensor can be addressed from several different perspectives [1, 2]; the purpose of this paper is to describe a novel system built at Miami University which utilizes UWB orthogonal frequency division multiplexing (OFDM) system architecture and wave-forming method. OFDM as a method of digital modulation is not a new technique – its concept was explored in 1960's by several researchers, e.g. [3]. However, it was not until the beginning of the 2000's that this technique and corresponding system architecture started being considered for wideband applications. There were two major reasons precluding UWB implementation of OFDM: Federal Communications Commission's (FCC) ban on commercial use of wide swaths of spectrum, which was lifted for extremely low-power signals in 2002; and unavailability of fast, inexpensive analog-to-digital (A/D) and digital-to-analog (D/A) converters [4], as they are significant components of an OFDM system determining its bandwidth. As soon as these two hurdles were overcome, UWB OFDM became a focus of R&D efforts in the industry and academia with an emphasis on commercial broadband communications [5, 6].

Implementation of OFDM signals and system architecture in radar, on the other hand, has not been as widely explored as in communications. Most notable research work concerning OFDM-coded radar signals is by Dr. Nadav Levanon, whose analyses of multicarrier phase coded (MCPC) radar signal performance were based on OFDM signal construction [7, 8]. Another study of OFDM-coded radar signals, published in [9], pointed out that these signals compare favorably to same-bandwidth LFM waveforms since range-Doppler coupling/ambiguity is much less pronounced in case of using OFDM signals. In [10] we also performed a simulation study of achieving SAR imaging with OFDM-coded waveforms based on conventional system architecture.

Despite fairly significant advantages – such as pulse diversity potential and dual-use system design – OFDM, and, in particular, UWB OFDM signal construction and system architecture were not widely considered for applications in radar. This paper is intended as initial analysis of such an application, examined from experimental perspective.

II. SYSTEM ARCHITECTURE AND SIGNAL DESIGN

The system is built as a short-range, X-band high-resolution radar and communication unit for possible implementation in airborne radar sensor networks. OFDM signal construction is performed in the digital block and the subsequent upconversion and amplification is performed in the analog front-end (AFE) portion, as shown in Fig. 1.

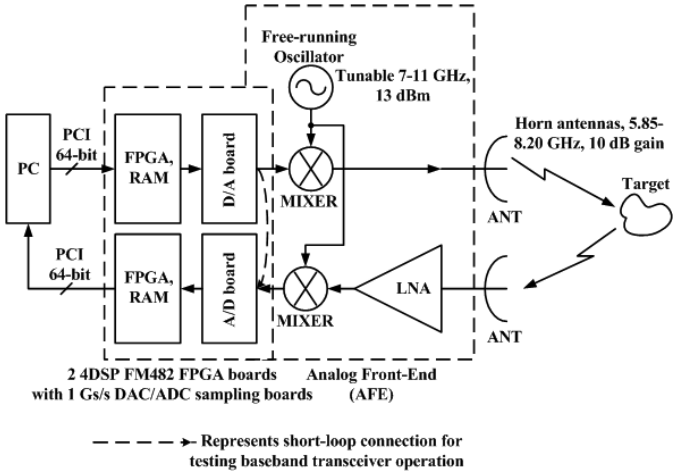

Figure 1. System block diagram

This work is supported by the U.S. Air Force Office of Scientific Research under Grant FA9550-07-1-0297.

A baseband OFDM signal is formed using N sub-bands centered at $k{\cdot}f_1$ sub-carrier frequencies (k=1, 2…N), where $f_1=F_s/(2N)$ and F_s is a sampling frequency of a D/A converter in OFDM radar transmitter. It follows then that the mathematical discrete spectrum of the signal will consist of $2N$+1 samples and the resultant time-domain vector will have the same number of points and it will also be symmetric with respect to its $(N+1)^{th}$ sample. The transmit time-domain signal $x(n)$ with $2N$+1 samples are shown in (1):

$$x(n)=\frac{1}{2N+1}\cdot\sum_{k=1}^{2N+1}X(k)\cdot e^{j2\pi\frac{(k-1)(n-1)}{2N+1}},\quad n=1...2N+1 \tag{1}$$

where $X(k)$ in our system are real-valued samples of the mathematical spectrum which are either radar signal codes, or data vector representation depending on the system functionality. In the receiver the conversion from received signal samples $x_R(n)$ to frequency-domain sample vector $X_R(k)$ is shown in (2):

$$X_R(k)=\sum_{n=1}^{2N+1}x_R(n)\cdot e^{-j2\pi\frac{k\cdot n}{2N+1}},\quad k=1...2N+1 \tag{2}$$

Equations (1)-(2) can also be interpreted as a transmit-receive pair, in which $x(n)$ from (1) is the baseband digital transmit signal form and $X_R(k)$ from (2) is the receive signal form used to extract target information if in radar mode, or decode the data message if in communications mode. In a general OFDM system $X(k)$ samples represent original data to be transmitted and $x(n)$ is created from $X(k)$ via inverse Fourier transform, implemented as IFFT in our platform.

After $x(n)$ is formed, it is sent to the D/A converter to create a voltage waveform $x(t)$:

$$x(t)=\begin{cases}\dfrac{1}{2N+1}\cdot\displaystyle\sum_{k=1}^{2N+1}X(k)\cdot e^{j2\pi\frac{(k-1)F_s}{2N+1}t}, & 0\le t\le\dfrac{2N}{F_s}\\ 0, & t>\dfrac{2N}{F_s}\end{cases} \tag{3}$$

which is then mixed with a 7.5 GHz carrier signal from the free-running oscillator to form a transmit signal sent to the antennas. The spectrum of this signal is shown in Fig. 2. System parameters are summarized in Table I.

TABLE I. UWB-OFDM SYSTEM PARAMETERS

Parameter	Value	Units
Baseband signal bandwidth	500	MHz
Transmitted signal bandwidth	7.0…8.0	GHz
Number of sub-bands in a pulse	Variable	
Transmit power, approximately	25	mW
Typical radar pulse length	129	ns
Typical symbol length per pulse	19	bits
Typical range for radar and communications	2…5	meter

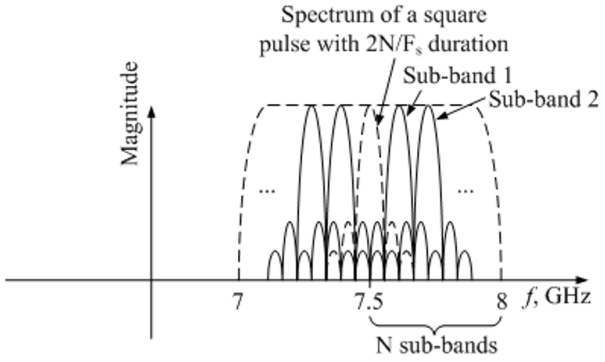

Figure 2. Schematic representation of the system transmit/receive spectrum

It should be noted that since the radar's transmitter operates in a pulsed mode, the emitted power estimate should be made using the entire pulse repetition interval (PRI). The appropriate provision for this type of measurements – and the waiver to the original rules – has been adopted by the FCC on March 10, 2005 [11]. According to this waiver, the original measurement procedure (which required the manufacturers to measure the power with the transmitter operating as if in continuous-wave mode) can result in "…measured emission levels that are greater than the UWB signal levels under actual operation." Thus, a more realistic approach to estimating a UWB system's transmit power was adopted (with the exception of 5030-5650 MHz band) – which allows for power estimation during normal device operation, i.e. within the entire PRI. Using this definition, we set the PRI to 50 μs and the typical radar pulse length to 129 ns, thus creating a 0.258% duty cycle in the normal operational mode. This configuration resulted in the estimated transmit power of approximately –42.9 dBm/MHz, which is in line with the FCC regulations for indoor systems.

III. RADAR CAPABILITY EXPERIMENTAL STUDY

The test objectives for radar functionality experiment were to construct a range profile for a multiple number of targets and determine the resolution of the current system. The targets used in experimentation were trihedral corner reflectors with 1-foot square sides. From [12] the radar cross-section (RCS) of a square-faced trihedral corner reflector is

$$\sigma=\frac{12\pi a^4}{\lambda^2}, \tag{4}$$

where a is the side length of the reflector and λ is the radar signal's wavelength, both in meters. This results in an RCS of approximately 200 m^2 at the carrier frequency of 7.5 GHz. Estimated signal power at the target is about −30 dBm, which is compliant with the FCC spectral mask for UWB-OFDM transmissions. It was also determined that a target placement of approximately 1.1 meters or more from the antennas would allow for far field testing. Indoor tests were conducted in the typical lab environment, schematically shown in Fig. 3.

Range reconstruction after receiving the reflected signal was performed using matched filtering implemented as either time-domain correlation, or frequency-domain multiplication [13]:

$$x_M(t) = \mathbb{F}^{-1}\left[X_R(\omega) X^*(\omega) \right], \quad (5)$$

where $x_M(t)$ is the range profile in time domain (or the output of a matched filter), $\mathbb{F}^{-1}$ denotes inverse Fourier transform operation and asterisk denotes complex conjugate. Time-domain base is then converted into distance and range resolution is defined as a minimum discernible difference between peaks in matched filter response corresponding to signals reflected from different targets. Evidently, theoretical range resolution is a function of the sampling rate of A/D converter in the receiver – the size of a range bin for our system is found as

$$\Delta r = \frac{c \cdot \left(\frac{1}{F_s} \right)}{2} = 0.15\ m\ , \quad (6)$$

which translates to the best theoretical range resolution between two target reflectors of $2\Delta r = 0.30$ m.

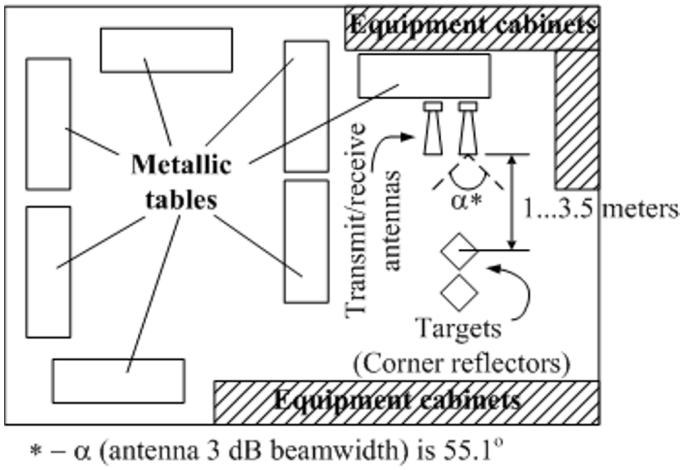

Figure 3. Laboratory setup where the radar experiments were conducted (not clutter-free environment).

Range profile experiments were performed for two-target scenario, in which, as shown in Fig. 3, corner reflectors were separated in range from the antennas. The reflectors were located at the same elevation as the antennas. The number of sub-bands for OFDM signal construction was chosen to be $N = 256$, resulting in 512 ns pulse duration, and the sub-band amplitude weights were assigned randomly as real-valued normally distributed numbers. Fig. 4(a)-(d) show the range profiles for the two target scenario corresponding to Table II. All of the range profiles are magnified at the peaks so the number of samples between peaks can be seen more clearly. To determine the actual target range we sent the transmit signal directly to the receiver using short-loop path, while simultaneously sending it through the radar AFE to the antennas. We then performed matched filtering of the transmitted and received signals using the first peak as the reference point, measuring the number of samples between the reference peak and the target peak. Using the expected number of time samples for the signal traveling from the antenna to the target we can determine the signal travel time through the radar AFE and cables by subtraction of the samples. Adopting this technique, we have determined that the front end delay is 26 samples or 26 nanoseconds.

TABLE II. TWO-TARGET RANGE PROFILE DATA

Fig. 5 graph	Actual distance, m (From antennas/From 1st target)	Recovered distance, m (From antennas/From 1st target)
(a)	1.85/0.28	1.95/0.30
(b)	2.00/0.43	2.10/0.45
(c)	2.16/0.59	2.25/0.60
(d)	2.61/1.04	2.70/1.05

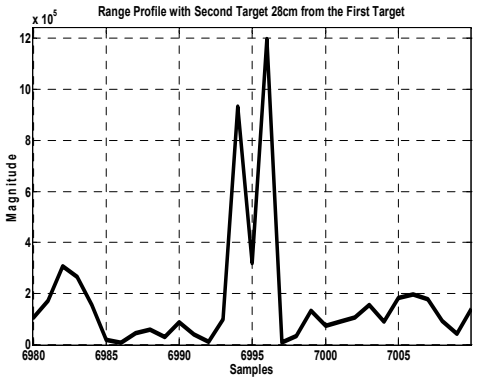

(a)

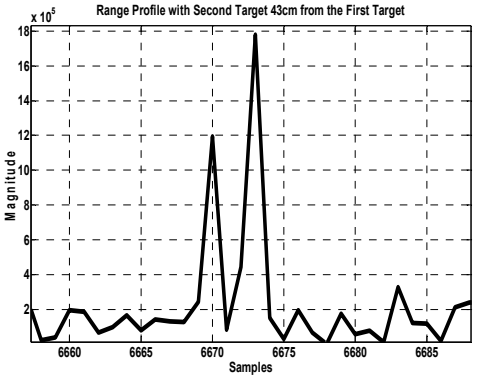

(b)

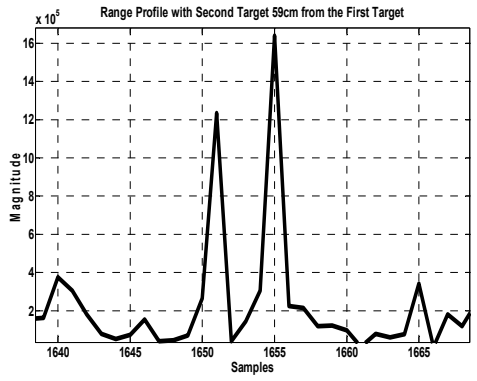

(c)

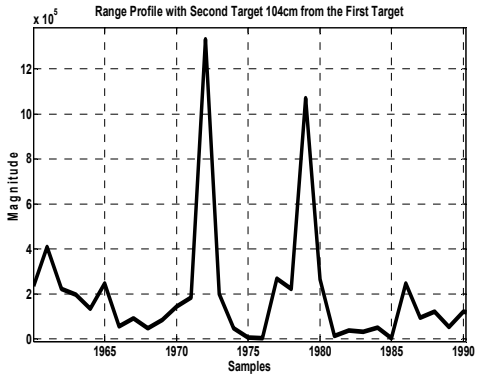

(d)

Figure 4. Two-target test result for a 256-sub-band OFDM signal with randomly distributed sub-band coefficients, with two targets being apart by: (a) 0.28 m; (b) 0.43 m; (c) 0.59 m; (d) 1.04 m.

IV. Data Communication Experimental Study

The goal of this experiment was to show that the designed system can be used as a broadband data communication device with no hardware adjustments. Communications using the radar requires the identification of which sub-bands are enabled upon receipt of the OFDM symbol. The transmission speed depends on the number of sub-bands (sub-channels) that can be simultaneously enabled. The B = 500 MHz bandwidth of the baseband signal is sub-divided into C sub-channels. The OFDM symbol is formed by taking the IFFT of the data vector encoded in frequency domain, forming a set of $2C$ samples. Since the symbol generation is software defined, the number of sub-channels may be dynamically set in real time to account for varying channel considerations. For the experiments in this section, the number of sub-channels was chosen to be 64. Thus, each OFDM symbol has length

$$L_{sym} = \frac{2 \cdot C}{2 \cdot B} = 128\,ns \tag{7}$$

The binary serial input data is divided into blocks of length C. Each block is encoded by mapping the block's bits onto the sub-channels of the OFDM symbol. The sub-channels were modulated using on-off keying (OOK) to facilitate easier data recovery. OOK encodes one bit per channel, so each input data block maps directly to one OFDM symbol. With all of the 64 sub-carriers enabled a maximum bit/symbol rate of 64 could be achieved. Experimentally it was found that many of the physical channels were susceptible to systemic in-band noise generated by the AFE, and thus a subset of size $C_{enabled}$ of the physical channels C was chosen to carry data during our tests. PAPR issues were mitigated by standard clipping techniques [14].

The guard interval between successive OFDM symbols was chosen to be 4 times the length of the typical delay spread of UWB signals in our environment [15], resulting in a guard interval length of L_{guard} = 200 ns.

The low L_{sym}/L_{guard} ratio infers an efficiency loss in data rate; however, the small L_{sym} was chosen to decrease the PRI for increased jamming resistance of system operation. The data rate of our system is then

$$R = \frac{C_{enabled}}{L_{guard} + L_{sym}} \tag{8}$$

Experimentally it was found that sub-channels in the 0-100 MHz range, as well as those near the sampling rate in 470-500 MHz range, interfered heavily with the operation of nearby sub-channels. This effect is due to signal distortion by the D/A and A/D conversions, and it is not an effect of the transmission channel. To reduce this ICI, guard bands equal to the width of a single channel were introduced to reduce the effect of energy spreading on adjacent bands. In addition, sub-carriers that were prone to ICI were not used for data transmission and were also treated as guard bands. This approach was found to be reasonably resilient to adjacent band ICI. Three configurations of enabled sub-channels were tested, as shown in Table III. Fig. 5 shows signal transmission and reception examples for the simplest case of two enabled sub-channels.

TABLE III. Sub-Channel Configurations

Config.	Enabled sub-channels	Total number of sub-channels	Resultant data rate, Mb/s
C1	16-60, even only	19	57
C2	10-60, even only	26	79
C3	0-64, even only	32	97

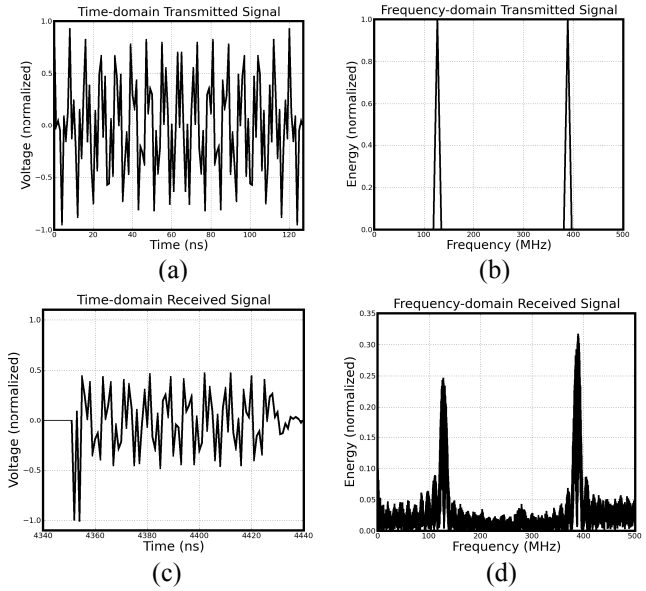

(a) (b)

(c) (d)

Figure 5. Example of signal generation, transmission and reception for communications: (a) Ideal signal generated in MATLAB; (b) Ideal signal's spectrum with two sub-channels enabled; (c) Received signal after down-conversion to baseband and 1 Gs/s sampling; (d) Received signal's computed spectrum.

By receiving a single OFDM symbol, our spectral resolution is one sample per sub-channel. Since the guard band width is exactly that of a sub-channel, we sample each guard

band. To recover the data in these configurations, the energy in enabled sub-channels can be compared to the energy in adjacent guard bands. To detect energy in the *i*th sub-channel S_i, the quantity

$$Q = \frac{2E(S_i) - E(S_{i-1}) - E(S_{i+1})}{2} \quad (9)$$

is evaluated using threshold detection, where *E(.)* denotes the energy in a sub-channel. To test the power limit performance, each of the sub-channel configurations from Table III was also implemented with a quarter of power through halving the sub-channel amplitudes; these configurations were denoted $C1_{low}$, $C2_{low}$ and $C3_{low}$. All communication experiments were performed in the same laboratory setting as radar experiments; the only difference was absence of targets and antenna arrangements in which transmit and receive antennas were facing each other. Several thousand pulse sequences were transmitted, received and analyzed for bit error ratio (BER) performance. The aggregate BER plot for all six configurations is shown in Fig. 6. It is seen that the lab range of 5 meters does not quite allow us to explore the distance limits of our data transmission scheme, as the BER mostly depends on the sub-channel configuration even for the low-power set.

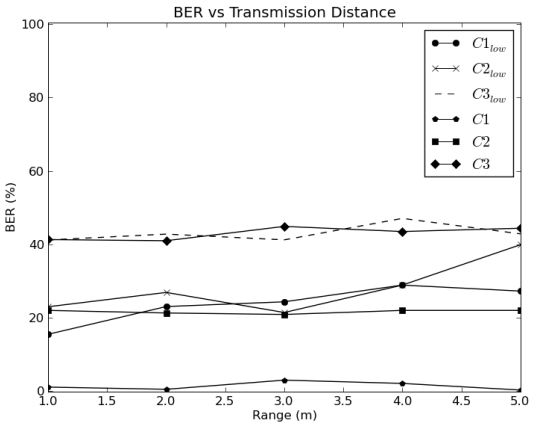

Figure 6. Bit error rate performance in six configurations.

The plot establishes C1 configuration – 57 Mb/s – as the only transmission scheme allowing below-5% BER performance over the maximum range from approximately 1 to 5 meters.

V. CONCLUSION

An experimental system based on OFDM architecture has been designed and built at Miami University. The system's useful bandwidth is 500 MHz, which allows it to perform as high-resolution radar with range resolution approximately 0.30 meter. The system can also be used as a communication unit with experimental data rate of 57 Mb/s enabling broadband communications. There are no required hardware alterations to make the system switch from radar to communications functionality and only minor software adjustments are necessary – thus providing seamless radar and data communications capability fusion. The system is also expected to possess good anti-jamming capabilities by employing pulse diversity due to the ability to change the number and composition of sub-carriers, as well as pulse width on a pulse-to-pulse basis. Using OFDM architecture and signal processing, which is heavily reliant on FFT/IFFT and high-speed sampling, allows for fast and relatively inexpensive system design. Implementation of such a system is targeted at low cost/weight airborne platforms in radar sensor network environments.

ACKNOWLEDGMENT

The authors are grateful to Jonathan Schuerger for range profile data collection.

REFERENCES

[1] *Sandia MiniSAR – Miniaturized Synthetic Aperture Radar*, Sandia National Laboratories, Albuquerque, NM. Available: http://www.sandia.gov/RADAR/minisar.html

[2] M. Edrich, "Ultra-lightweight synthetic aperture radar based on a 35 GHz FMCW sensor concept and online raw data transmission," in *IEE Proc. Radar, Sonar Navig.*, vol. 153, pp. 129–134, Apr. 2006.

[3] R. Chang and R. Gibby, "A theoretical study of performance of an orthogonal multiplexing data transmission scheme," *IEEE Trans. Communications,* vol. 16, no. 4, pp. 529–540, Aug. 1968.

[4] Bin Le, T. W. Rondeau, J. H. Reed, and C. W. Bostian, "Analog-to-digital converters," *IEEE Signal Processing Mag.*, vol. 22, no. 6, pp. 69–77, Nov. 2005.

[5] A. Batra, J. Balakrishnan, G. R. Aiello, J. R. Foerster, and A. Dabak, "Design of a multiband OFDM system for realistic UWB channel environments," *IEEE Trans. Microwave Theory and Tech.*, vol. 52, no. 9, Part 1, pp. 2123–2138, Sep. 2004.

[6] C. Snow, L. Lampe, and R. Schober, "Performance analysis of multiband OFDM for UWB communication," in *Proc. 2005 IEEE Int. Conf. Communications*, Seoul, Korea, 2005, vol. 4, pp. 2573–2578.

[7] N. Levanon, "Multifrequency complementary phase-coded radar signal," in *IEE Proc. Radar, Sonar Navig.*, vol. 147, no. 6, pp. 276–284, Dec. 2000.

[8] N. Levanon and E. Mozeson, *Radar Signals.* Hoboken, NJ: Wiley-Interscience, 2004, ch. 11.

[9] G. E. A. Franken, H. Nikookar, and P. van Genderen, "Doppler tolerance of OFDM-coded radar signals," in *Proc. 2006 European Radar Conf.*, Manchester, UK, 2005, pp. 108–111.

[10] D. S. Garmatyuk, "Simulated imaging performance of UWB SAR based on OFDM," in *Proc. 2006 IEEE Int. Conf. on Ultra-Wideband*, Waltham, MA, 2006, pp. 237–242.

[11] "FCC adopts waiver of its emission measurement procedures for ultra-wideband transmission systems," *FCC News Release*, Mar. 10, 2005. Available: http://fjallfoss.fcc.gov/edocs_public/attachmatch/DOC-257308A1.pdf

[12] E. F. Knott, M. T. Tuley, and J. F. Schaeffer, Radar Cross-Section. Raleigh, NC: SciTech Publishing, 2006.

[13] M. Soumekh, Synthetic Aperture Radar Signal Processing. New York: Wiley, 1999.

[14] Xiaodong Li, L.J. Cimini, Jr., "Effects of clipping and filtering on the performance of OFDM," in Proc. *1997 IEEE 47th Vehicular Technology Conf.*, Phoenix, AZ, 1997, vol.3, pp.1634–1638.

[15] T.Jamsa, V.Hovinen, A.Karjalainen, J. Iinatti, "Frequency dependency of delay spread and path loss in indoor ultra-wideband channels," in Proc. *2006 Institution of Engineering and Technology Seminar on Ultra Wideband Syst., Tech. and App.*, London, UK, 2006, pp.254–258.